Pyridyl-benzimidazole derivatives decorated with phenylazo substituents and their low-spin iron(ii) complexes: a study of the synthesis, structure and photoisomerization

Jakub Orvoš, Róbert Fischer, Barbora Brachňaková, Ján Pavlik, Ján Moncoľ, Alexandra Šagátová, Marek Fronc, Jozef Kožíšek, Lucie Routaboul, Azzedine Bousseksou, et al.

Pyridyl-Benzimidazole Derivatives Decorated with Phenylazo Substituents and their Low-Spin Iron(II) Complexes: Synthesis, Structural and Photoisomerization Study

Jakub Orvoš,[a] Róbert Fischer,[a]* Barbora Brachňaková,[b,d] Ján Pavlik,[b] Ján Moncoľ,[b] Alexandra Šagátová,[b] Marek Fronc,[c] Jozef Kožíšek,[c] Lucie Routaboul,[d] Azzedine Bousseksou [d] and Ivan Šalitroš[b,e,f]*

a) Department of Organic Chemistry, Faculty of Chemical and Food Technology, Slovak University of Technology in Bratislava, Bratislava SK-81237, Slovakia, **e-mail:* robert.fischer@stuba.sk
b) Department of Inorganic Chemistry, Faculty of Chemical and Food Technology, Slovak University of Technology in Bratislava, Bratislava SK-81237, Slovakia. **e-mail:* ivan.salitros@stuba.sk
c) Department of Physical Chemistry, Faculty of Chemical and Food Technology, Slovak University of Technology in Bratislava, Bratislava SK-81237, Slovakia
d) LCC, CNRS & Université de Toulouse, 205 route de Narbonne, 31077 Toulouse, France
e) Department of Inorganic Chemistry, Regional Centre of Advanced Technologies and Materials, Faculty of Science, Palacký University, 17. listopadu 12, 771 46 Olomouc, Czech Republic
f) Central European Institute of Technology, Brno University of Technology, Purkyňova 123, 61200 Brno, Czech Republic

Graphical abstract

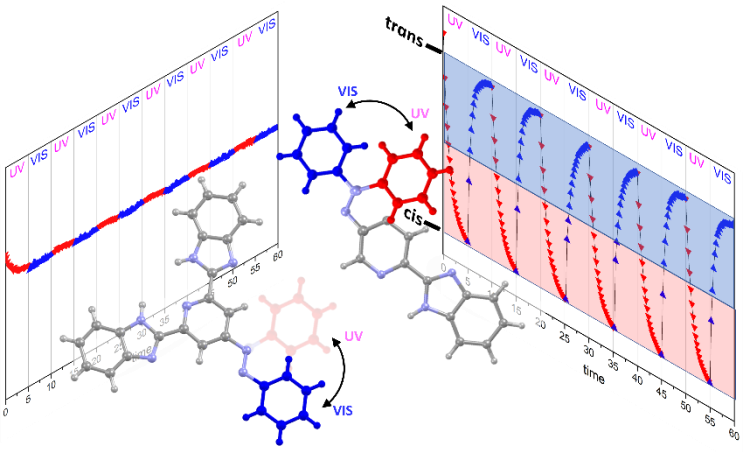

Series of phenylazo substituted pyridyl-benzimidazole ligands and their ferrous complexes have been prepared. Photoirradiation experiments allowed to investigate *E-Z* isomerisation of ligands, which was further rationalized by computational study.

Abstract

The series of phenylazo-substituted derivatives of pyridyl-benzimidazoles **L1**-**L5** has been synthesized by modified Mills reaction and their structural, spectral and photoswitching properties were investigated. NMR spectroscopy and single-crystal X-ray diffraction analysis of desired compounds confirmed their *E* conformation. The light-induced *E*↔*Z* (also called as *trans*↔*cis*) isomerization was monitored by UV-VIS and ^{1}H NMR spectroscopy that revealed reversible photochromic behavior governed by first-order kinetics. By the help of state-of-the-art *meta-dynamics* simulations (iMTD-GC) and *ab-initio* calculations (CASSCF-NEVPT2 and STEOM-DLPNO-CCSD) the analysis of electronic structures of ligands was possible which helped to explain bland *E-to-Z* conversion of **L1** and pronounced switching of **L2**-**L5** ligands. Furthermore, the computational studies identified the active wavelengths of *E-to-Z* conversion and allowed to assess the mechanisms of photoisomerization. Additionally, ligands **L1** and **L2** were used for the preparation of four ferrous coordination compounds **C1**-**C4** in which the structural and magnetic investigations confirmed the permanent low-spin state and diamagnetic behavior in the solid state. On the other hand, dissolved compounds **C1** and **C2** are high-spin at room temperature and their blue light irradiation causes the decomplexation instead of desired *E*-to-*Z* isomerization.

Introduction

The azobenzene-based derivatives have attracted great interest due to their photoresponsive switchable properties that can be applied in biological systems,[1] optical switches,[2] molecular machines[3] or data storage devices.[4] Generally, the transition from *E* (*trans*) to *Z* (*cis*) conformation is activated by UV-VIS light irradiation,[5] electrostatic stimulation[6] or with mechanical stress,[7] while the backward *Z*-to-*E* reaction occurs either upon the visible light irradiation or spontaneously in the dark due to the thermodynamic stability of *E* isomer. In azobenzene, which is an archetypal member of this group, the first intensive absorption appears around 320 nm due to $\pi\rightarrow\pi^*$ transition (abbr. $\pi\pi^*$) and the weak absorption around 450 nm is assigned to symmetry-forbidden $n\rightarrow\pi^*$ transition (abbr. $n\pi^*$).[5] The $\pi\pi^*$ absorption is dominant for both conformers and its intensity decreases by about one order of magnitude with *E*-to-*Z* photoisomerization. On the other hand, the intensity of the $n\pi^*$ band is unchanged or even sometimes increases upon the transformation to *Z* form.[8-10] Thus, the mentioned excited states $S_1(n\pi^*)$ and $S_2(\pi\pi^*)$ of azobenzene moiety must be populated when the transformation from one isomeric form to another occurs.[9] Detailed insights into the mechanisms of the photoisomerization of azobenzene and its analogues has been elucidated through computational studies.[11,12] Despite the fact that the first report of *Z*-to-*E* interconversion was published more than eighty years ago,[13] the mechanism of this reversible isomerization is still not completely clear and there are tentatively proposed routes of transformation which aim the rotation, inversion, concerted inversion or inversion assisted rotations of aromatic benzene rings with respect to the azo-bond.[10-12,14] Kinetics of photoisomerization process, quantum yield of photoconversion as well as the lifetime of the metastable *Z* form are often affected by experimental conditions (temperature,[15] pressure,[16] solvent[17]) or by structural modification.[18,19]

From the coordination chemistry point of view, the introduction of phenylazo (PA) moiety on the ligand systems is an interesting strategy for the development of transition metal coordination compounds with light tunable properties, since the electronic structure of ligand is different when the light switchable moiety is in *E* or in *Z* conformation.[20] In particular, different conformation of PA substituents affects the ligand field strength,[21] which can be employed for modulation of properties of magnetically bistable single molecule magnets[22] or spin crossover[23] complexes by light. In this context, the family of pyridyl-benzimidazole derivatives is an interesting class of bidentate or tridentate N-donor ligands with molecular structure, that allows a rationalized introduction of substituents capable for instance to elevate the axial magnetic anisotropy in corresponding Co(II) complexes and to enhance the slow relaxation of magnetization.[24] In the same vein, the substituted pyridyl-benzimidazole ligands can allocate the thermal spin crossover of corresponding ferrous complexes into the room temperature or to above room temperature region and promote the photoinduced spin state switching.[25] One of the most successful reports on the Ligand-Driven Light-Induced Spin Change (LD-LISC)[21] active systems concerns the mononuclear Fe(II) complex with bidentate pyridyl-benzimidazole ligands bearing the PA substituents introduced on the benzimidazole moiety.[23a] LD-LISC effect brought about reversible photoinduced *E*-to-*Z* changes accompanied by significant decrease of π-back-donation properties, responsible for a decrease of the ligand field at constant temperature. Indeed, authors achieved the partial *E*-to-*Z* switching in the solution, which was accompanied by increase of high-spin state mole fraction at isothermal conditions.

Inspired by the results of Hasegawa and co-workers,[23a] herein we report on the preparation, structural and spectral properties of bidentate and tridentate pyridyl-benzimidazole derivatives containing PA substituents introduced on the pyridine ring of ligand skeleton (Figure 1). The molecular design of ligands assumed, that PA group introduced directly onto pyridine ring might affect the electronic structure of central atom more effectively comparing to a Hasegawa's bidentate ligand with PA introduced on the distant phenyl ring of benzimidazole part.[23a] The gram-scale synthesis of one bis(benzimidazole)pyridine and four pyridyl-benzimidazole derivatives decorated by PA was optimized in several synthetic steps and molecular structures were confirmed by spectral and X-ray diffraction analysis. Additionally, tridentate ligands were used for preparation of four low-spin Fe(II) coordination compounds. *E*-to-*Z* photoswitching for all ligands has been accomplished in solution at room temperature and the rate of the isomerization process was established. A metadynamic simulation of finite-temperature NMR spectra helped to prove successful photoswitching of ligands in solution while the state-of-the-art computational methods CASSCF-NEVPT2 and STEOM-DLPNO-CCSD were used to calculate the potential energy scans and absorption spectra, respectively, in order to assess the possible isomerization mechanism and explain different switching capability of the ligands.

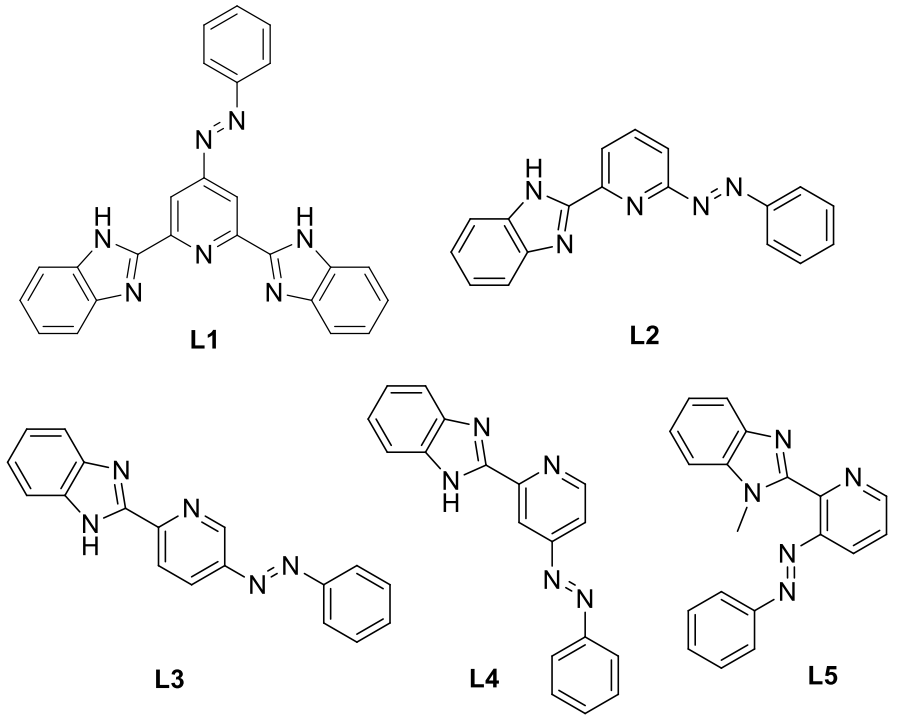

Figure 1. Molecular structures of reported tridentate (**L1**, **L2**) and bidentate (**L3**-**L5**) ligands. Tridentate ligands have been used for the synthesis of iron(II) coordination compounds C**1**-C**4** of general formula $[Fe(L1)_2]A_2$ or $[Fe(L2)_2]A_2$ (where A^-=BF_4^-, ClO_4^- and $CF_3SO_3^-$).

Results and discussion

Syntheses and structural characterizations

Synthetic procedures, characterization of reported compounds and technical details of the experimental and theoretical investigation are described in supplementary information (SI). The strategy for the synthesis of PA-pyridine-substituted compounds was based on the Mills reaction of amino-substituted (2-benzimidazolyl)pyridines with nitrosobenzene.[26] The

benzimidazole ring was formed by acid-catalyzed cyclization of *N*-(2-aminophenyl)pyridine carboxamides obtained from the amidation reaction of the corresponding pyridine carboxylic acids with *o*-phenylenediamine. The preparation of **L2** and **L3** has been reported very recently by some of us,[27] and here we discuss their synthetic protocols together with other phenylazo functionalized derivatives of pyridyl-benzimidazole.

The synthetic route for the preparation of tridentate compound **L1** is outlined in Scheme 1 and complete NMR characterization of each intermediate as well as final organic compounds is viewed on Figure S1 (see SI). 4-Azidopyridine derivative **1b** was synthesized in 95 % yield from commercially available dimethyl 4-chloropyridine-2,6-dicarboxylate (**1a**) using slightly modified literature procedure.[28] The basic hydrolysis of **1b** with lithium hydroxide in aqueous THF gave dicarboxylic acid **1c** in 98 % yield. Following amidation reaction with *o*-phenylenediamine (3 eq) employing *O*-(benzotriazol-1-yl)-*N*,*N*,*N'*,*N'*-tetramethyluronium tetrafluoroborate (TBTU, 2.2 eq) in the presence of DIPEA (4 eq) in DMF under highly diluted conditions afforded diamide **1d** in very good 79 % yield.[29] Another activating agents such as EDCI,[30] DCC,[31] or CDI[32] provided very low or no yield of **1d**. Catalytic hydrogenation of **1d** in the presence of Pd/C in MeOH gave amino derivative **1e** in 95 % yield.[33] Subsequent treatment of this compound with acetic acid at 100 °C produced NH_2-bis(benzimidazole)pyridine **1f** in excellent 93 % yield. [29b] First, the Mills reaction of **1f** with nitrosobenzene was examined in acetic acid as the solvent and catalyst, as well at 80 °C.[34] Unfortunately, only trace amount of the product was detected in the reaction mixture even after longer reaction time. This problem was overcome by the reaction in basic conditions of aqueous sodium hydroxide in pyridine.[35] The modified reaction conditions were required due to decreased reactivity of NH_2-bis(benzimidazole)pyridine compound **1f**. The concentrated 50 % aq. NaOH (10 eq) caused the formation of biphasic reaction mixture with pyridine and together with phase transfer catalyst TBAB (0.2 eq) significantly accelerated the reaction at 50 °C. Such arrangement of the experiment was necessary to avoid rapid nitrosobenzene degradation (3 eq, added in two portions) in strongly alkaline conditions and to improve the yield of target ligand **L1** up to 75 % yield. Finally, the optimized synthesis of **L1** was performed on a gram scale (3.51 g) in a total yield of 40 %, starting from dimethyl 4-chloropyridine-2,6-dicarboxylate (**1a**) (5 g), without using the chromatographic purification of intermediates and the final product (see SI, Experimental section). It is worth noting that **L1** undergoes partial isomerization at ambient conditions, since the small amount of *Z*-**L1** was identified in the ^{1}H NMR spectra of solution exposed to daylight for several days (for benzimidazole protons 6´-H and 7´-H of *Z*-isomer at 7.20-7.16 and 7.14-7.10 ppm, with respect to *E* isomer in the region between 7.40-7.29 and 7.83-7.75 ppm, respectively; Figure S2a).

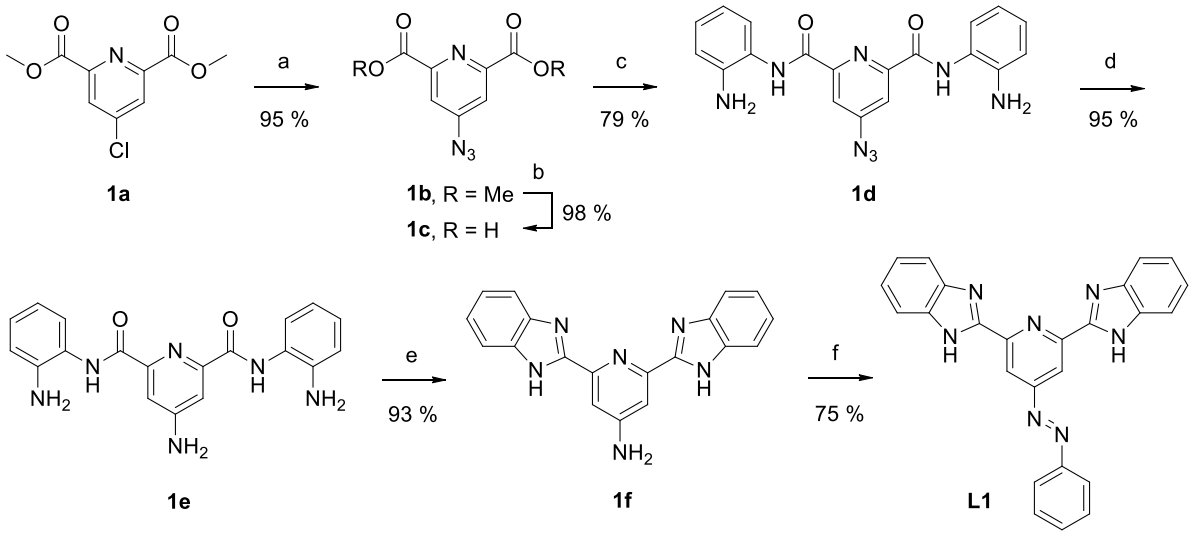

Scheme 1. Synthesis of ligand **L1**. Reaction conditions: (a) NaN_3, DMF, 50 °C, 24 h; (b) $LiOH \cdot H_2O$, THF/H_2O (1:1), r.t., 20 min; (c) *o*-phenylenediamine, TBTU, DIPEA, DMF, r.t., 20 h; (d) H_2 (4 bar), Pd/C (10 wt%), MeOH, r.t., 2 h; (e) AcOH, 100 °C, 1 h; (f) nitrosobenzene, 50 % aq. NaOH, TBAB, pyridine, 50 °C, 3.5 h.

Ligands **L2-L5** were prepared according to the above-mentioned procedure in three steps with 42–52 % overall yields, starting from commercially available amino-substituted picolinic acids **2a**, **3a**, **4a** and **5a** (Scheme S2, Figure S1). Surprisingly, the Mills reaction of amino derivative **5c** with nitrosobenzene did not lead to formation of the desired product even at higher temperatures (80–100 °C) and gradual degradation of both the starting aminopyridine and nitrosobenzene was observed. This problem has been successfully overcome by regioselective *N*-methylation of **5c** with methyl iodide in the presence of K_2CO_3 resulting to the (*N*-methyl)benzimidazole derivative **5d** (Scheme S3).[36] Next, the reaction of **5d** with nitrosobenzene resulted to the final ligand **L5** in 62 % yield after crystallization from *o*-xylene. Also **L5** undergoes partial reversible *Z*-to-*E* isomerization upon ambient conditions.[37] This behavior was clearly identified by two-dimensional TLC analysis on silica gel as two similarly colored spots with significantly different R_f values (in CH_2Cl_2/MeOH, 96:4; $R_f(E) = 0.29$, $R_f(Z) = 0.44$), that interconverted quickly during the procedure. The mixture of *Z/E* isomers in the solution was proved by NMR spectroscopy due to the change of chemical shifts of the 4-H pyridine ring proton signals (for *Z*-isomer at 6.94 ppm with respect to *E* isomer at 8.18 ppm, Figure S2b).[38]

Molecular structures of targeted organic ligands **L1**-**L5** consist of pendant PA moiety attached to pyridine ring of bis(benzimidazole)pyridine (**L1**) or pyridyl-benzimidazole (**L2**-**L5**) ligand skeleton in the positions 6´ (**L2**), 5´ (**L3**), 4´ (**L1** and **L4**) and 3´ (**L5**). This structural motive was confirmed by ^1H and ^{13}C NMR spectroscopy (Figure S1 and S2), by FTIR (Figure S3) and **L1**, **L4** and **L5** were characterized also by single-crystal X-ray diffraction analysis (Figure 2 and S4), which revealed their *E* conformation in the solid state. Compounds crystallize in triclinic *P*-1 (**L1**·DMF and **L4**) or monoclinic $P2_1/c$ (**L5**) space group with four (**L1**·DMF and **L4**) and two (**L4**) molecules of ligands included in the unit cell. Further crystallographic parameters are shown in SI (Table S1). Tridentate ligand **L1** crystallizes from DMF solution with co-crystalized solvent molecule (**L1**·DMF). Benzene ring of PA group is turned by 16° with respect to the plane of pyridine ring of bis(benzimidazole)pyridine moiety. Similarly, in

L4 are the corresponding phenyl rings of PA group also turned by 33° and 14°. However, this angle is significantly deformed in nonplanar **L5** (≈ 63°) due to the intramolecular repulsions caused by the introduction of imidazole moiety. All three structures contain also non-covalent contacts. Imidazole N-H groups of **L1** form hydrogen bonds with oxygen atom of DMF (O1···N7=2.891(4) Å; O1···N10=3.184(4) Å; Figure S4a). Additionally, molecules of **L1** are interconnected *via* weak π···π contacts formed between phenyl rings of PA and benzimidazolyl moieties with average distances about 3.91 Å (Figure S4a). In the structure of **L4**, the ligand molecules are interconnected through hydrogen bonds created between imidazole nitrogen atoms (N1-H···N6=2.896(2) Å and N5-H···N2=2.890(2) Å). This interconnection is responsible for the formation of 1D supramolecular arrangement of ligand molecules along the *a*-*c* plane (Figure S4b). Nonplanar molecular structure of **L5** shows out-of-plane orientation of aromatic units with respect to the pyridyl plane, which allows the formation of π···π contacts between benzene rings of PA and benzimidazole groups with distances longer than 4 Å (Figure S4c).

Furthermore, we report on four ferrous coordination compounds **C1**-**C4** prepared by the complexation of tridentate ligands **L1** and **L2** with ferrous salts in acetonitrile-ethanol (**C1**), nitromethane-ethanol (**C2**) and in ethanol (**C3** and **C4**) yielding coordination compounds $[Fe(L1)_2](BF_4)_2 \cdot H_2O$ (**C1**), $[Fe(L1)_2](CF_3SO_3)_2 \cdot 0.75CH_3CH_2OH \cdot CH_3NO_2$ (**C2**), $[Fe(L2)_2](BF_4)_2 \cdot C_2H_5OH \cdot 3H_2O$ (**C3**) and $[Fe(L2)_2](ClO_4)_2 \cdot 2.2H_2O$ (**C4**). Their molecular structures are viewed on Figure 2 and Figure S5 and selected structural parameters are listed in Table S2 (SI). Isostructural compounds **C1** and **C2** crystalize in triclinic space group *P*-1, while **C3** and **C4** crystalize in monoclinic space group $P2_1/n$. Molecular structures of reported coordination compounds contain one complex dication, two anions and corresponding lattice solvent molecules. In each compound, the complex dication consists of two tridentate ligands coordinated with Fe(II) central atom. In **L2**, the PA substituent is introduced on the position 2´ of pyridine ring allowing the participation of azo bond on the coordination with central atom. Therefore, the **L2** acts as a tridentate ligand and binds the metal center *via* three nitrogen donor atoms of imidazole, pyridine and azo moiety. Obviously, such tridentate coordination prevents the ability of *E*-*Z* photoisomerization in the **C3** and **C4**. Coordination polyhedron of each complex cation contains six N-donor atoms set coordinated with Fe(II) metal center and its shape can be expressed as a distorted octahedron. At 100 K, Fe-N bond distances vary in the range 1.87-2.00 Å (Table S3) typical for the low-spin state of the Fe(II) metal center. This statement is supported also by metric distortion parameters Σ and Θ,[39] calculated from angles of coordination polyhedra. Σ and Θ parameters acquire the values in the range 79 – 109° and 259 – 328°, respectively, (Table S3) which are typical for the low-spin state of Fe(II) metal center in the family of ferrous complexes with tridentate aromatic ligands.[39c] Additionally, the magnetic measurements have confirmed the diamagnetic low-spin state properties of **C1**-**C4** up to 400 K (Figure S6).

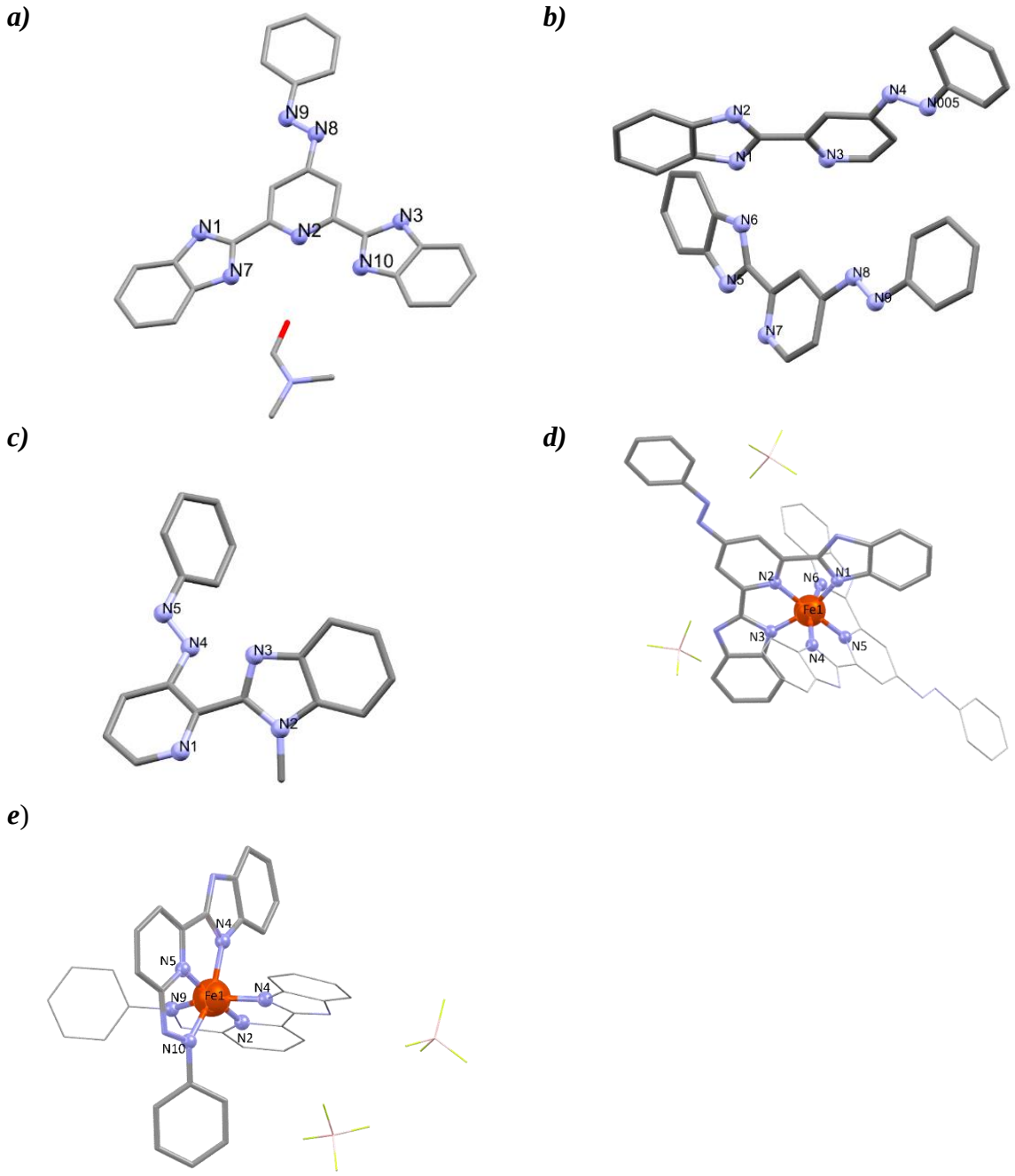

Figure 2 The molecular structure of a) **L1**, b) **L4**, c) **L5**, d) **C1** and e) **C3**. The hydrogen atoms and lattice solvent molecules are omitted for clarity. Color code: C- grey; N-blue; O-red; Fe-orange; B- pink; F-light green.

Photoisomerization experiments

In order to characterize the photoswitching properties of **L1**-**L5** and coordination compounds **C1**-**C4**, the electron absorption spectroscopy was carried out in ethanolic solution at room temperature (Figure S7). Generally, the compounds containing azo bonds show a pronounced $\pi\pi^*$ absorption band in the region 300 – 370 nm (ground singlet state to second excited singlet state, $S_2 \leftarrow S_0$) and much weaker $n\pi^*$ band (ground singlet state to first excited singlet state, $S_1 \leftarrow S_0$) in the region 400 – 450 nm.[13,40] In the studied series of ligands, the maxima of $\pi\pi^*$ bands are found at 319 nm for **L1**, 317 nm for **L2**, 369 nm for **L3**, 311 nm for **L4** and 300 nm

L5 (Figure 3a, Figure S7, Table 2 *vide infra*). The similar and simpler analogues of reported ligands, n-phenylazopyridines (n=2-4), show the $\pi\pi^*$ transitions of PA group also around 320 nm.[41] So the absorptions of **L3** and **L5** are obviously out of the expected range. The highest energy of $\pi\pi^*$ transition in **L5** could be explained by the suppressed π-conjugation throughout the molecule of ligand, which is the consequence of its non-planar structure (*vide supra*). On the contrary, the *para* orientation of PA and benzimidazole substituents promotes the π-conjugation over the planar structure of ligand **L3**, which leads to the red shift of its $\pi\pi^*$ transition.[42] Comparatively weaker $n\pi^*$ absorption bands of **L1**-**L5** occur between 385-460 nm (inserted graphs in Figure S7).

Continuous UV irradiation of **L1**-**L5** in ethanol solution caused the decrease of $\pi\pi^*$ absorption bands and partial increase of the $n\pi^*$ absorption bands. Such spectral changes are typical for the *E*→*Z* isomerization. When photostationary state has been reached, the UV light was switched off and immediate exposure of the blue light (λ_{exc}= 450 nm) caused the reverse increase of $\pi\pi^*$ bands indicating the backward photoconversion to *E* isomer. The change of absorbance at corresponding maximum over the consecutive six cycles of UV (*E*→*Z*) and VIS (*Z*→*E*) irradiation confirmed reversibility of photoswitching in **L1**-**L5** (Figure 3b). Furthermore, the multiple cycling of UV/blue light irradiation was repeated several times without noticeable fatigue. Under the UV irradiation, the smallest decrease of absorbance was found for **L1**, while the largest one for **L3**. The low yield of *Z*-**L1** was only slightly improved by the irradiation with 405 nm laser light (Figure S9a, *vide infra*), which has been attributed to antenna-like effect stabilizing the electron density on bis(benzimidazole)pyridine moiety in **L1** excited states (*vide infra*).

In general, the kinetics of *E*↔*Z* photoisomerization can be deduced from the time dependent absorbance measurements (Figure S8 and S9, Table 1). The rate constants of **L1**-**L5** were calculated using the following equation

$$kt = ln\frac{(A_0 - A_{inf})}{(A_t - A_{inf})} \quad (1)$$

where *k* - rate constant of the isomerization, *t* - time, A_0 - the absorbance maximum of $\pi\pi^*$ band before irradiation, A_t - the absorbance maximum at given time and A_{inf} - absorbance maximum at the end of photochemical reaction.[42] The experimental rate constants $k_{(E\rightarrow Z)}$ were calculated for the first decrease of absorbance upon UV irradiation and vary in the narrow range 10.0×10^{-3} s^{-1} -15.1×10^{-3} s^{-1} (Table 1, Figure S8). Next, the thermal stability of photoproducts was studied at ambient temperature (Figure S9). The solution was irradiated with UV light (or with 405 nm laser light for solution of **L1**) for 5 minutes until the photostationary state was reached and the backward *Z*→*E* isomerization was monitored in the dark. These measurements revealed that photoproducts start to decay in several minutes (Figure S9). Similar to the other (phenylazo)pyridine derivatives,[41] the irradiated solutions relax back to thermodynamically stable *E* conformations and reach full back conversion at the hours scale (Figure S9). Among the ligands under the study, the highest rate constants of *Z*-to-*E* transformation are observed for **L1** (1.43×10^{-4} s^{-1}) and **L4** (2.0×10^{-4} s^{-1}), which both contains the PA group introduced on the pyridine ring in the position 4´. On the other hand, the remaining ligands **L2, L3** and **L5** with PA substituent introduced on position 6´, 5´ and 3´, respectively, have smaller and rather comparable $k_{(Z\rightarrow E)}$ rate constants (0.32×10^{-4} s^{-1} -0.46×10^{-4} s^{-1}; Table 1)

Table 1 Kinetic data for **L1-L5**.

Ligand	**L1**	**L2**	**L3**	**L4**	**L5**
$k_{(E\rightarrow Z)}$ / 10^{-3} s^{-1}	15.1	11.9	14.2	10.0	10.1
$\tau_{(E\rightarrow Z)}$ / s	66.2	84.0	70.4	100.0	99.0
$k_{(Z\rightarrow E)}$ / 10^{-4} s^{-1}	1.43	0.33	0.32	2.0	0.46
$\tau_{(Z\rightarrow E)}$ / s	6993	30303	31250	5000	21739

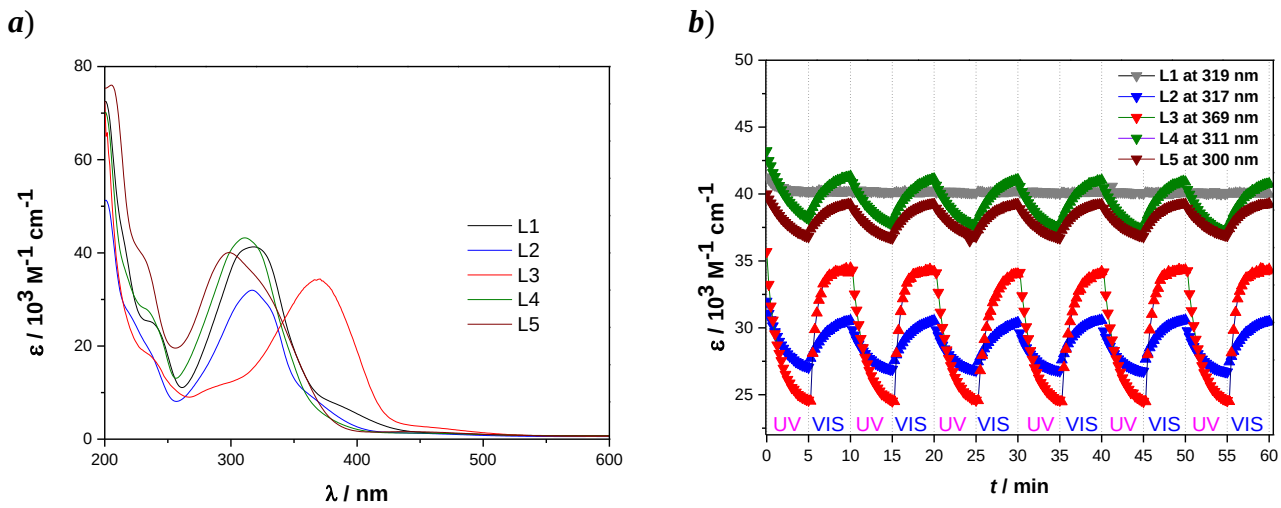

Figure 3 ***a)*** UV-VIS spectra of reported ligands in ethanol solution. ***b)*** Reversible interconversion between the *E* and *Z* isomers of reported ligands in ethanol solution under UV and blue (λ_{exc}= 450 nm) light irradiation shown as the time dependence of change in molar absorption coefficient ε at corresponding maxima. Data were collected every 15 seconds over 5 minutes upon UV or blue irradiation and the photoswitching was repeated 6 times.

^{1}H NMR spectroscopy of DMSO-d_6 (**L1**) or methanol-d_4 solutions (**L2-L5**) was also employed for the detection of *Z* isomers (Figure S10). The sharp and well separated signals of *Z* isomers in the 6.3-8.6 ppm range were observed after 5 minutes of UV light irradiation. New-resolved signals assigned to pyridyl and/or ortho-phenyl protons allowed quantitative evaluation of formed *Z* isomers showing a yield of 50 % (**L2**), 38 % (**L3**), 18 % (**L4**) and 20 % (**L5**). Weak and overlaying signals of *Z*-**L1** prevent reliable calculation of conversion yield and its value is estimated between 15-20 %. A *state-of-the-art* composite computational method was also employed, which allowed to predict the finite-temperature real-solution ^{1}H NMR spectra for both geometric isomers. In fact, the most of the works which aim at prediction of NMR spectra deals with molecular geometry optimized at absolute zero temperature in vacuum. Simulation of real experimental conditions requires sorting of enormous number of sampled isomers and rotamers which leads to so-called *nuclear permutation problem*.[44] This obstacle has been solved in a very recent series of works by Grimme et al.[44-46] Having reliable set of molecular geometries, the chemical shielding constants and spin-spin coupling constants were calculated using the meta-GGA DFT functional TPSS,[47] which performs very well in this sake[48] (for more information see Computational Details). A very good agreement with the experiment can be concluded, which confirms the photoswitching event and clarifies the corresponding spectral shifts of *E* and *Z* form, respectively (Figure S10).

Furthermore, UV-VIS spectroscopy investigation of **C1**-**C4** revealed that all complex compounds show intensive $\pi\pi^*$ absorption bands around 330 nm (Figure 4), which are red-shifted comparing to the electron absorption spectra of free ligands **L1** and **L2**. The red shift may be explained by the coordination of ligands with Fe(II) ions, which is also evidenced by the presence of less intensive MLCT bands above 600 nm. Both absorption bands supposed to change upon the isomerization and therefore can serve as sensitive indicators of switching in the molecular systems.[49] Although uncoordinated ligand **L2** shows *E*-*Z* photoisomerization, its photoswitching in complex compounds **C3** and **C4** is hindered by the coordination of azo-bond with Fe(II) central atom.

On the other hand, compounds **C1** and **C2** containing non-coordinated PA group were submitted for the investigation of *E*↔*Z* photoisomerization in the same way as uncoordinated ligands **L1**-**L5** (*vide supra*). We assumed that light-induced geometry changes of **L1** could modulate spin state through increasing and decreasing π-back-bonding character of coordinated ligand **L1** in *E* and *Z* conformations, respectively.[49] Initially, the ethanol solutions of **C1** and **C2** were irradiated by UV (long pass UV filter, 150 W halogen lamp) and blue light (450 nm band pass filter, 150 W halogen lamp) in four cycles. Unfortunately, the *E*-to-*Z* isomerization of **L1** under these conditions is relatively poor in both, coordinated and non-coordinated form (Figure 3) and therefore no changes in the electronic properties of the metal center are expected. Surprisingly, experiments carried out with 405 nm laser light revealed notable decrease of MLCT bands (≈ 720 nm) and increase of ππ* bands within 1 hour of irradiation at room temperature (Figure S11), which is the expected change for the low-spin→high-spin transition. Generally, the MLCT absorption band of low-spin state located in the VIS region is more intensive comparing to high-spin compound, and therefore the spin transition of Fe(II) complexes causes the decrease of MLCT band due to the enlarged metal-ligand distances.[50] On the other hand, the *Z*-to-*E* back conversion has not occurred either upon 460 nm light irradiation or after keeping solutions in the dark at room temperature for several hours. In order to explain observed spectral changes, we measured the magnetic susceptibility of **C1** and **C2** in DMSO-d_6 solution (Evans method,[51] Figure S12). Comparing to the low-spin diamagnetic solid-state behavior (*vide supra*), both dissolved compounds are paramagnetic and their room temperature χT values suggest the complete (**C1**; $\chi T \approx 3.7$ cm^3 K mol^{-1}) or almost complete (**C2**; $\chi T \approx 2.75$ cm^3 K mol^{-1}) high-spin state. Further magnetic measurements upon the increase of temperature or upon the irradiation haven't indicated any significant changes in the magnetic properties of both complexes. Additionally, no change in ^{1}H NMR spectra of **C1** and **C2** has been observed after the irradiation of their solutions. Thus, with respect to the detected high-spin state behavior of **C1** and **C2** in solution, the decrease of MLCT band and increase of ππ* bands upon the laser light irradiation is most probably related with the decomposition of complexes. The attempts to activate *E*-to-*Z* photoisomerization in the solid state were also largely unsuccessful. The long-term room temperature irradiation (365 nm LED, 375 nm laser) of **C1** in KBr pellet monitored by FTIR spectroscopy also did not reveal any signature of solid-state isomerization (Figure S13). Such inactivity of photoswitching might be associated with the large structural changes through isomerization in the crystal structure.

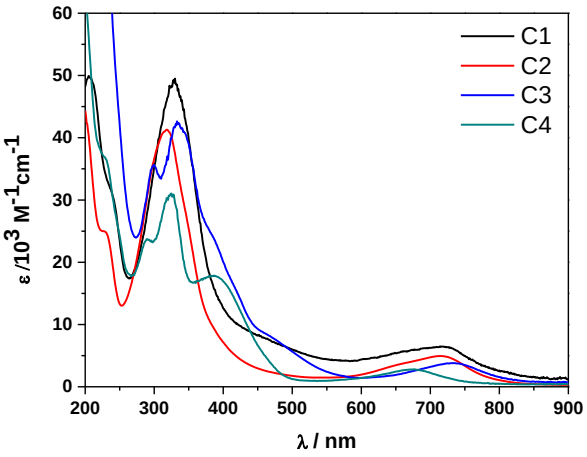

Figure 4 UV-VIS spectra of **C1** – **C4** dissolved in ethanol.

Computational study

To get a more complete picture on the switching, potential energy surface (PES) scan along the dihedral angle -CNNC- was computed for **L1**-**L5**. In this calculation, first the rotation around the bond in discrete steps was imposed upon the molecule and the geometry of each step was optimized. Secondly, for each geometry the SA-CAS[4,3]SCF method[51] was used, i.e. the energy of six lowest energy states was obtained by allowing four electrons of azo bond to occupy three molecular orbitals: bonding π, antibonding π^* and nonbonding n. In the final step, the energy of each state was improved by NEVPT2 method,[53] which counts in the correlation interaction from all other electrons (for more information see Computational Details). Resulting PES scan profiles are displayed in Figure 5 and Figures S14-S17 and show very similar features for all molecules. In accordance with expectation, the calculation predicts that the *E* isomer is thermodynamically more stable for all systems with relatively high activation barrier preventing fast thermal back switching at ambient conditions.

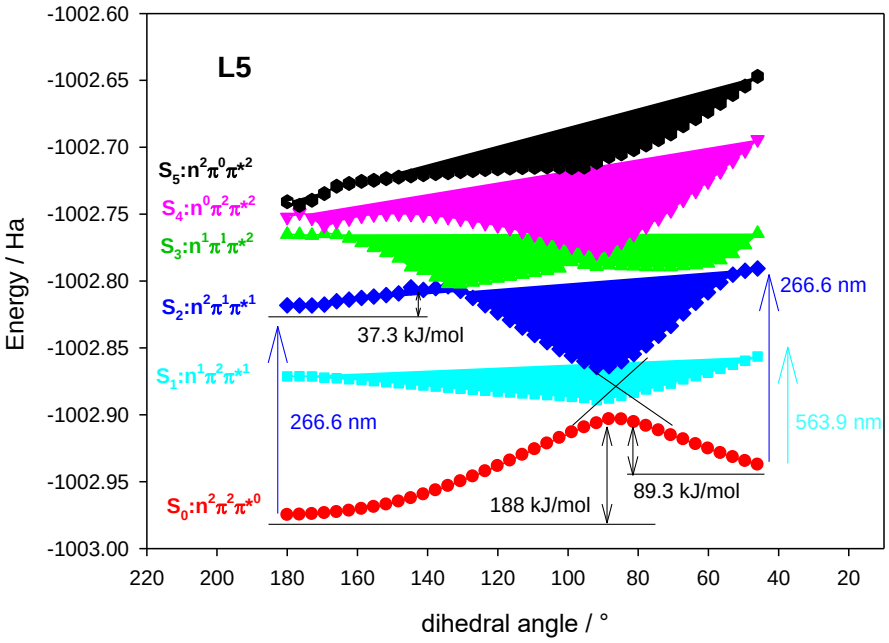

Figure 5 PES scan with respect to –CNNC– dihedral angle for **L5**.

Based on the PES scan profiles, the standard mechanism of light-induced rotational isomerization in azobenzene[11] and its derivates[54] can be assumed also in this class of compounds. According to that, the *E* isomer is expected to absorb primarily the UV radiation thanks to the symmetrically allowed transition from ground singlet state to the second excited singlet state ($S_2 \leftarrow S_0$, $\pi\pi^*$) transition and to much lower extent the visible blue light corresponding to symmetrically forbidden transition to first excited singlet state ($S_1 \leftarrow S_0$, $n\pi^*$). Nevertheless, some portion of molecules in S_1 state can be created also under UV radiation thanks to S_1/S_2 conical intersection seam corresponding to bending across the CNN bending mode.[11] Inspection of orbitals in the state S_2 showed that its electronic configuration can be expressed as $n^2\pi^1\pi^{*1}$ for every molecule, i.e. the bond order between nitrogen atoms in the azo-group is diminished and allows torsional rotation of the -CNNC- link.

Table 2 Comparison of experimental and calculated $\pi\pi^*$ excitation wavelengths in nm of *E* isomers of **L1-L5**.

Compound	$\lambda_{exp.}$/nm	SA-CASSCF-NEVPT2	STEOM-DLPNO-CCSD
***E*-L1**	319	300	310
***E*-L2**	317	295	323
***E*-L3**	369	317	346
***E*-L4**	311	296	306
***E*-L5**	300	267	314

The striking difference in yield of *E*-to-*Z* conversion as well as reversibility of photoswitching between the system **L1** and **L2-L5** (Figure 3) motivated us to inspect the possible reasons of such behavior. A promising new method called DLPNO-STEOM-CCSD for inspection of excited states was used.[55] It enables calculation of electronic spectra at the level of the quantum chemistry golden standard method *coupled-cluster singles-doubles* (CCSD) with much more affordable scaling.[56] The resulted predicted wavelengths of dominant absorption of *E* isomer are collected in Table 2 and Figure S7 together with values extracted from PES scans and from experiment. As can be seen, the agreement with experiment for all ligands outperforms the former SA-CASSCF-NEVPT2 strategy and gives us confidence in conclusion on electronic structure acquired from DLPNO-STEOM-CCSD. For this purpose, the Natural Transition Orbitals (NTOs) related to the dominant absorption of both isomers were inspected (Figure 6, Figure S18). Apparently, *E*-**L1** possesses by far lowest contribution of $\pi\pi^*$ transition to the dominant absorption out of all ligands. In other words, comparatively high portion of the transition occurs within the huge bis(benzimidazole)pyridine moiety and the order of the azo-bond is not sufficiently decreased. One can therefore conjecture that the -CNNC- bond rotation in *E*-**L1** is relatively ineffective despite successful photoexcitation.

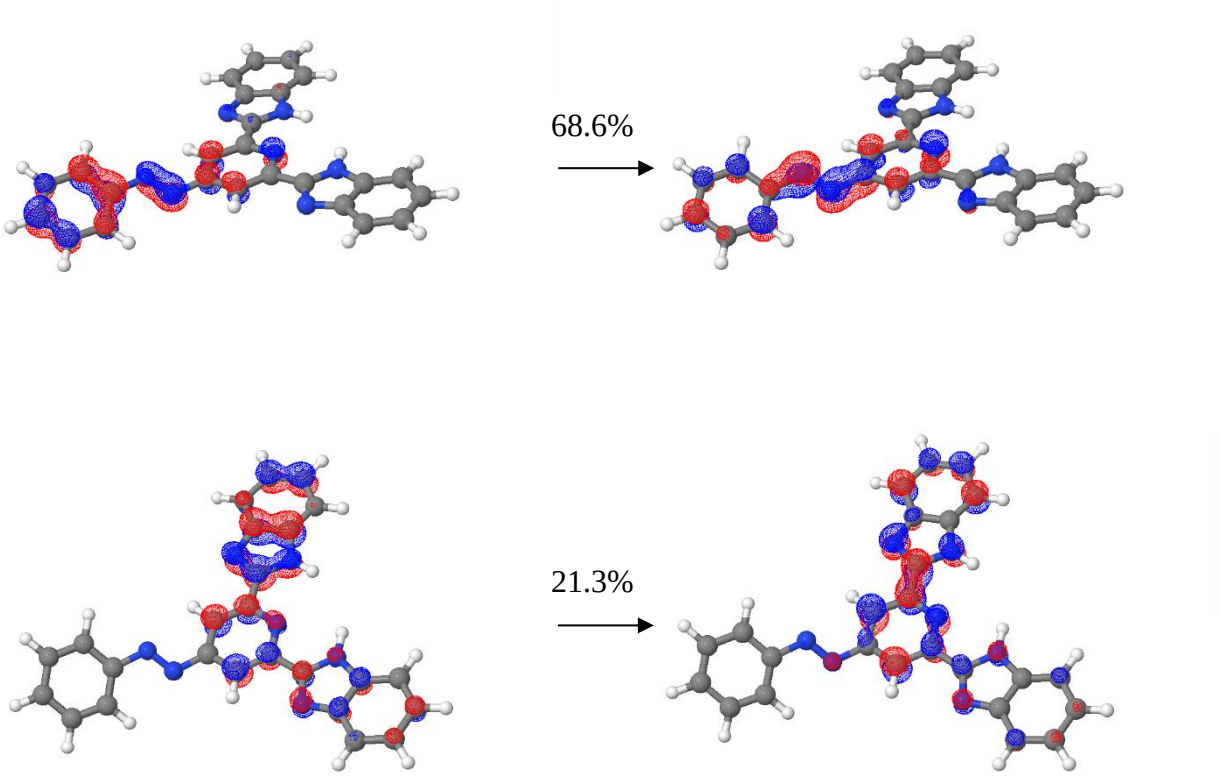

Figure 6 Natural transition orbitals extracted from STEOM-DLPNO-CCSD calculation for the most intensive transition in *E*-**L1.**

Summary
We report the synthesis of five novel pyridyl-benzimidazole ligands decorated by photoswitchable PA substituent. Their photoswitching has been successfully observed by the solution irradiation with the UV or blue laser light and the backward transformation to *Z* isomer has been achieved by visible light irradiation or by thermal conversion in the dark at ambient temperature. Although the conversion from *E* to *Z* conformer is less than 50 %, the light induced isomerization is reversible in several cycles, that makes it attractive as a building block for the construction of molecular switches. The kinetic studies indicate that isomerization is rather independent of the topology of PA substituent introduced on the pyridine ring. Simulated NMR spectra at real conditions support the assumption of successful photoswitching. Calculated PES scans bear features observed for the well described azobenzene, suggesting thus that the mechanism of photoisomerization is similar in **L1-L5**. On the other hand, huge aromatic segments appeared as counterproductive components in design of novel photoswitches, as they can make the isomerization mechanism ineffective. Furthermore, four ferrous coordination compounds have been synthetized from ligands **L1** and **L2**, which coordinate metal ion in tridentate fashion. While the complexes prepared from **L2** contain coordinated PA group blocked with respect to photoisomerization, the complexes with ligand **L1** have the PA substituent free to isomerize. However, their blue or UV light irradiation has been innocent with respect to the isomerization in the solid state and caused the decomposition of complexes in the solution. Additionally, it is important to note that all remaining ligands **L3-L5** are also used for the preparation of coordination compounds and study of their optical and magnetic properties in terms of LD-LISC effect is currently under the progress.

Conflicts of interest
There are no conflicts to declare.

Acknowledgements

Authors acknowledge Mrs. Laure Vendier for the single crystal X-ray diffraction experiments and structure refinement of compound **C3**. Slovak grant agencies APVV-18-0197, APVV-18-0016, APVV-19-0087, VEGA 1/0029/22, KEGA 018-STU-4 are acknowledged for the financial support. We acknowledge financial support from the Grant Agency of the Czech Republic (GAČR 22-23760S). I.Š. acknowledges the financial support from institutional sources of the Department of Inorganic Chemistry, Palacký University in Olomouc. JP acknowledges HPC center at STU (SIVVP project, ITMS code 26230120002, funded by the European region development funds, ERDF) and prof. Radovan Herchel from the Department of Inorganic Chemistry, Palacký University in Olomouc for making his computational resources available. BB would like to thank for financial contribution from the STU Grant scheme for Support of Young Researchers. This article was written thanks to generous support through the Operational Program Integrated Infrastructure for the project: " Strategic research in the field of SMART monitoring, treatment and preventive protection against coronavirus (SARS-CoV-2) " , Project no. 313011ASS8, co-financed by the European Regional Development Fund.

References

1. a) R. J. Mart, R. K. Allemann, *Chem. Comm.* **2016**, *52*(83), 12262–12277; b) M. Dommaschk, M. Peters, F. Gutzeit, C. Schütt, C. Näther, F. D. Sönnichsen, S. Tiwari, C. Riedel, S. Boretius, R. Herges, *J. Am. Chem. Soc.* **2015**, *137*(24), 7552–7555;
2. a) L. Zhang, J. Pan, C. Gong, A. Zhang, *J. Mat. Chem. C*. **2019**, *7*(34), 10663–10671; b) S.H. Ryu, M. J. Gim, W. Lee, S. W. Choi, D. K. Yoon, *ACS applied materials & interfaces* **2017**, *9*(3), 3186–3191; c) T. Ikeda, O. Tsutumi, *Science* 1995, 268, 1873-1875.
3. a) T. Muraoka, K. Kinbara, T. Aida, *Nature* **2006**, *440*, 512–515. b) M. Hammerich, R. Herges, *J. Org. Chem.* **2015**, *80*, 11233–11236.
4. Z. F. Liu, K. Hashimoto, A. Fujishima, *Nature* **1990**, 347, 658-660.
5. a) S. Kawata, Y. Kawata, *Chem. Rev.* **2000**, *100*, 1777–1788; b) D. Kim, K. Jeong, *Liq. Cryst. Today* **2019**, *28*, 34–45, DOI: 10.1080/1358314X.2019.1653588.
6. a) J. Henzl, M. Mehlhorn, H. Gawronski, K.-H. Rieder and K. Morgenstern, *Angew. Chem., Int. Ed*. **2006**, *45*, 603–606; b) X. Tong, M. Pelletier, A. Lasia, Y. Zhao, *Angew. Chem., Int. Ed*. **2008**, *47*, 3596–3599.
7. R. Turansky, M. Konopka, N. L. Doltsinis, I. Stich, D. Marx, *Phys. Chem. Chem. Phys*. **2010**, *12*, 13922–13932.
8. a) H. Rau Azo Compounds, p. 165-188 in Photochromism: Molecules and Systems (Eds.: H. Durr, H. Bouas-Laurent), Elsevier 2003 ISBN: 0-444-51322-1 b) P. Klán, *J. Wirz, Photochemistry of Organic Compounds*, Wiley-VCH, Weinheim, **2009**.
9. P. Bortolus, S. Monti, *J. Phys. Chem.* **1979**, *83*, 648–652.
10. a) E. Merino, M. Ribagorda, *Beilstein J. Org. Chem.* **2012**, *8*, 1071–1090; b) S. Crespi, N. A. Simeth, B. König, *Nat. Rev. Chem.* **2019**, *3*, 133–146; c) F. A. Jerca, V. V. Jerca, R. Hoogenboom, *Nat.Rev.Chem.* **2022** *6***,** 51–69.
11. a) R. J. Maurer, K. Reuter, *J. Chem. Phys.* **2011**, *135*, 224303; b) J. Casellas, M. J. Beapark, M. Reguero, *Chem. Phys. Chem.* **2016**, *17*, 3068–3079; c) A. Nenov, R. Borrego-Varillas, A. Oriana, L. Ganzer, F. Segatta, I. Conti, J. Segarra-Marti, J. Omachi, M. Dapor, S. Taioli, C. Manzoni, S. Mukamel, G. Cerullo, M. Garavelli, *J. Phys. Chem. Lett.* **2018**, *9*, 1534–1541; d) F. Segatta, A. Nenov, S. Orlandi, A. Arcioni, S. Mukamel, M. Garavelli, *Faraday Discuss* **2020**, *221*, 245; e) I. C. D. Merritt, D. Jacquemin, M. Vacher, *Phys. Chem. Chem. Phys.* **2021**, *23*, 19155–19165; f) J. R. Rouxel, D. Keefer, F. Aleotti, A. Nenov, M. Garavelli, S. Mukamel, *J. Chem. Theory Comput.* **2022** *18*, 605–613.
12. H. M. D. Bandarra, S. C. Burdette, *Chem. Soc. Rev.* **2012**, *41*, 1809–1825.
13. G. S. Hartley, *Nature* **1937**, *140*, 281.
14. a) H. Rau, E. Lueddecke, *J. Am. Chem. Soc.* **1982**, *104*, 1616–1620; b) C. R. Crecca, A. E. Roitberg, *J. Phys. Chem. A* **2006**, *110*, 8188–8203; c) J. L. Magee, W. Shand, Jr., H. Eyring, *J. Am. Chem. Soc*. **1941**, *63*, 677–688; d) D. Y. Curtin, E. J. Grubbs, C. G. McCarty, *J. Am. Chem. Soc.* **1966**, *88*, 2775–2786.
15. S. Samai, D. J. Bradley, T. L. Y. Choi, Y. Yan, D. S. Ginger, *J. Phys. Chem. C* **2017**, *121*, 6997−7004.
16. T. Moldt, D. Przyrembel, M. Schulze, W. Bronsch, L. Boie, D. Brete, C. Gahl, R. Klajn, P. Tegeder, M. Weinelt, *Langmuir* **2016**, *32*, 10795−10801.
17. G. Angelini, N. Canilho, M. Emo, M. Kingsley, C. Gasbarri, *J. Org. Chem*. **2015**, *80*, 7430−7434.
18. E. Wagner-Wysiecka, N. Łukasik, J. F. Biernat, E. Luboch, *J. Incl. Phenom. Macrocycl. Chem.* **2018**, *90***,** 189–257.
19. N. A. Simeth, S. Crespi, M. Fagnoni. B. König, *J. Am. Chem. Soc.* **2018**, *140*, 2940−2946.
20. a) Y. Gao, V. Walter, M. J. Ferguson, R. R. Tykwinski, *Chem. Eur. J.* **2020**, *26*, 16712; b) S. Kume, M. Kurihara, H. Nishihara, *Chem. Commun.* **2001**, 1656–1657; c) A. Telleria, P. W. N.

M. van Leeuwen, Z. Freixa, *Dalton Trans*. **2017**, *46*, 3569; d) G. Markiewicz, A. Walczak, F. Perlitius, M. Piasecka, J. M. Harrowfield, A. R. Stefankiewicz, *Dalton Trans.* **2018**, *47*, 14254.

21. a) B. Brachňaková, I. Šalitroš, *Chem. Pap.* **2018**, *72***,** 773–798; b) M. M. Khusniyarov, *Chem. Eur. J.* **2016**, *22*, 15178–15191.
22. T. K. Prasad, G. Poneti, L. Sorace, M. J. Rodriguez-Douton, A-L. Barra, P. Neugebauer, L. Costantino, R. Sessoli, A. Cornia, *Dalton Trans*. **2012**, *41*, 8368–8378.
23. a) Y. Hasegawa, S. Kume, H. Nishihara, *Dalton Trans*. **2009**, 280–284; b) S. Thies, H. Sell, C. Schütt, C. Bornholdt, C. N ther, F. Tuczek, R. Herges, *J. Am. Chem. Soc.* **2011**, *133*, 16243–16250; c) A. Bannwarth, S. O. Schmidt, G. Peters, F. D. Sönnichsen, W. Thimm, R. Herges, F. Tuczek, *Eur. J. Inorg. Chem.* **2012**, 2776–2783.
24. a) B. Brachňaková, S. Matejová, J. Moncoľ, R. Herchel, J. Pavlik, E. Moreno-Pineda, M. Ruben, I. Šalitroš, *Dalton Trans.* **2020**, *49*, 1249; b) J. Juráková, J. Dubnická Midlíková, J. Hrubý, A. Kliuikov, V. Tadeu Santana, J. Pavlik, J. Moncoľ, E. Čižmár, M. Orlita, I. Mohelský, P. Neugebauer, D. Gentili, M. Cavallini, I. Šalitroš, *Inorg. Chem. Front*. **2022**, *9*, 1179.
25. a) B. Brachňaková, J. Adamko Kožíšková, J. Kozisek, E. Melníková, M. Gál, R. Herchel, T. Dubaj, I. Šalitroš, *Dalton Trans.* **2020**, *49*, 17786–17795. b) R. Boča, M. Boča, L. Dlháň, K. Falk, H. Fuess, W. Haase, W. Linert, B. Papánková, R. Werner, *Inorg. Chem.* **2001**, *40*, 3025–3033;
26. E. Merino, *Chem. Soc. Rev.* **2011**, *40*, 3835–3853.
27. L. Masaryk, J.Orvoš, K. Soczyska, R. Herchel, J. Moncol, D. Milde, P. Halaš, R. Krikavova, P. Koczurkiewicz, E. Pekala, R. Fischer, I. Salitros, I. Nemec and P. Starha, Inorg. Chem. Front., 2022, in press DOI: 10.1039/D2QI00535B.
28. Z. E. A. Chamas, X. Guo, J.-L. Canet, A. Gautier, D. Boyer, R. Mathiou, *Dalton Trans.* **2010**, *39*, 7091–7097.
29. a) S.-Y. Han, Y.-A. Kim, *Tetrahedron* **2004**, *60*, 2447–2467; b) Y. Fang, H. Zhou, Q. Gu, J. Xu, *Eur. J. Med. Chem.* **2019**, *167*, 133–145; c) G. Liu, B. T. Campbell, M. W. Holladay, J. M. Ford Pulido, H. Hua, D. Gitnick, M. F. Gardner, J. James, M. A. Breider, D. Brigham, B. Belli, R. C. Armstrong, D. K. Treiber, *Med. Chem. Lett.* **2012**, *3*, 997–1002.
30. M. Kortelainen, A. Suhonen, A. Hamza, I. Pápai, E. Nauha, S. Yliniemelä-Sipari, M. Nissinen, P. M. Pihko, *Chem. Eur. J.* **2015**, *21*, 9493–9504.
31. K. Ghosh, S. Kumar, R. Kumar, U. P. Singh, *J. Organomet. Chem.* **2014**, *750*, 169–175.
32. a) W. A. Kinney, N. E. Lee, R. M. Blank, C. A. Demerson, C. S. Sarnella, N. T. Scherer, G. N. Mir, L. E. Borella, J. F. DiJoseph, C. Wells, *J. Med. Chem.* **1990**, *33*, 327–336; b) I.-R. Jeon, T. D. Harris, *Chem. Commun.* **2016**, *52*, 1006–1008.
33. P. Gandhi, B. Huang, J. C. Gallucci, J. R. Parquette, *Org. Lett.* **2001**, *3*, 3129–3132.
34. a) H. Kamogawa, T. Kasai, T. Andoh, T. Nakamura, *Bull. Chem. Soc. Jpn.* **1987**, *60*, 2905–2909; b) C. W. Grathwol, N. Wössner, S. Swyter, A. C. Smith, E. Tapavicza, R. K. Hofstetter, A. Bodtke, M. Jung, A. Link, *Beilstein J. Org. Chem.* **2019**, *15*, 2170–2183.
35. a) K. Suwa, J. Otsuki, K. Goto, *Tetrahedron Lett.* **2009**, *50*, 2106–2108; b) A. Bannwarth, S. O. Schmidt, G. Peters, F. D. Sönnichsen, W. Thimm, R. Herges, F. Tuczek, *Eur. J. Inorg. Chem.* **2012**, *16*, 2776–2783; c) K.-S. Cheon, R. A. Cox, S.-R. Keum, E. Buncel, *J. Chem. Soc., Perkin Trans. 2* **1998**, 1231–1239; d) S. Oldknow, D. Rota Martir, V. E. Pritchard, M. A. Blitz, C. W. G. Fishwick, E. Zysman-Colman, M. J. Hardie, *Chem. Sci.* **2018**, *9*, 8150–8159; e) A. Telleria, J. Pérez-Miqueo, A. Altube, E. García-Lecina, A. de Cózar, Z. Freixa, *Organometallics* **2015**, *34*, 5513–5529.
36. G. Balboni, R. Guerrini, S. Salvadori, L. Negri, E. Giannini, S. D. Bryant, Y. Jinsmaa, L. H. Lazarus, *J. Med. Chem.* **2005**, *48*, 8112–8114.

37. a) P. J. Coelho, C. M. Sousa, M. C. R. Castro, A. M. C. Fonseca, M. M. M. Raposo, *Optical Materials* **2013**, *35*, 1167–1172, and references cited therein; b) A. M. Sánchez-León, P. Cintas, M. E. Light, J. C. Palacios, *Eur. J. Org. Chem.* **2020**, 2827–2841.
38. a) J. Berthet, L. Agouridas, S. Chen, H. Allouchi, P. Melnyk, B. Champagne, S. Delbaere, *Dyes and Pigments* **2019**, *171*, 107666; b) A. Islam Sk, K. Kundu, P. K. Kundu, *Chem. Eur. J.* **2020**, *26*, 4214–4219; c) J. G. Schantl, P. Margaretha, *Helv. Chim. Acta* **1981**, *64*, 2492–2494.
39. a) P. Guionneau, M. Marchivie, G. Bravic, J.-F. Létard, D. Chasseau, *Top. Curr. Chem.* **2004**, *234*, 97–128; b) M. A. Halcrow, *Coord. Chem. Rev.* **2009**, *253*, 2493–2514; c) M. A. Halcrow, *Chem. Soc. Rev.* **2011**, *40*, 4119–4142.
40. Y. Xu, Ch. Gao, J. Andréasson, M. Grøtli, *Org. Lett.* **2018**, *20*, 4875–4879.
41. a) M. Nakagawa, M. Rikukawa, M. Watanabe, K. Sanui, N. Ogata, *Bull. Chem Soc. Jpn.* **1997**, *70*, 737–744; b) J. Otsuki, K. Narutaki, *Bull. Chem Soc. Jpn.* **2004**, *77*, 1537–1544.
42. Dong. M., Babalhavaeji, A., Samanta, S., Beharry, A. A., Wooley, G. A., Acc. Chem. Res., 2015, 48, 2662-2670.
43. P. Sierocki, H. Maas, P. Dragut, G. Richardt, F. Vogtle, L. De Cola, F. Brouwer, J. I. Zink, *Phys. Chem. B* **2006**, *110*, 24390–24398.
44. S. Grimme, C. Bannwarth, S. Dohm, A. Hansen, J. Pisarek, P. Pracht, J. Seibert, F. Neese, *Angew. Chem. Int. Ed.* **2017**, *56*, 12485–12491.
45. a) C. Bannwarth, S. Ehlert, S. Grimme, *J. Chem. Theory Comput.* **2019**, *15*, 1652–1671; b) C. Bannwarth, E. Caldeweyher, S. Ehlert, A. Hansen, P. Pracht, J. Seibert, S. Spicher, S. Grimme, *WIREs Comput. Mol. Sci.* **2020**, e01493; c) P. Pracht, F. Bohle, S. Grimme, *Phys. Chem. Chem. Phys.* **2020**, *22*, 7169–7192; d) S. Grimme, *J. Chem. Theory Comput.* **2019**, *15*, 2847–2862; e) S. Grimme, F. Bohle, A. Hansen, P. Pracht, S. Spicher, M. Stahn, *J. Phys. Chem. A* **2021**, *125*, 4039–4054; f) J. G. Brandenburg, C. Bannwarth, A. Hansen, S. Grimme, *J. Chem. Phys.* **2018**, *148*, 064104; g) S. Grimme, A. Hansen, S. Ehlert, J.-M. Mewes, *J. Chem. Phys.* **2021**, *154*, 064103; h) S. Grimme, J. G. Brandenburg, C. Bannwarth, A. Hansen, *J. Chem. Phys.* **2015**, *143*, 054107; i) E. Caldeweyher, S. Ehert, A. Hansen, H. Neugebauer, S. Spicher, C. Bannwarth, S. Grimme, *J. Chem. Phys.* **2019**, *150*, 154122; j) F. Jensen *J. Chem. Theory Comput.* **2015**, *11*, 132–138; k) F. Jensen, *J. Chem. Theory Comput.* **2006**, *2*, 1360–1369.
46. J. Tomasi, B. Mennucci, R. Cammi, *Chem. Rev.* **2005**, *105*, 2999–3094.
47. J. M. Tao, J. P. Perdew, V. N. Staroverov, and G. E. Scuseria, *Phys. Rev. Lett.* **2003**, *91*, 146401.
48. M. T. de Oliveira, J. M. A. Alves, A. A. C. Braga, D. J. D. Wilson, C. A. Barboza, *J. Chem . Theory Comput.* **2021**, *17*(11), 6876–6885.
49. K. Takahashi, Y. Hasegawa, R. Sakamoto, M. Nishikawa, S. Kume, E. Nishibori, H. Nishihara, *Inorg. Chem.* **2012**, *51*(9), 5188–5198.
50. S. De, L.-M. Chamoreau, H. El Said, Y. Li, A. Flambard, M.-L. Boillot, S. Tewary, G. Rajaraman, R. Lescouëzec, *Front. Chem.* **2018**, 6, 326.
51. a) D. F. Evans, J. Chem. Soc. 1959, 2003-2005; b) E. M. Schubert, J. Chem. Ed. 69, 62-62.
52. P. A. Malmqvist, B. O. Roos, *Chem. Phys. Lett.* **1989**, *155*(2), 189−194.
53. a) C. Angeli, R. Cimiraglia, J.-P. Malrieu, *Chem. Phys. Lett.* **2001**, *350*(3-4), 297−305; b) C. Angeli, R. Cimiraglia, S. Evangelisti, T. Leininger, J.-P. Malrieu, *J. Chem. Phys.* **2001**, *114*(23), 10252−10264; c) C. Angeli, R. Cimiraglia J.-P. Malrieu, *J. Chem. Phys.* **2002**, *117*(20), 9138−9153.
54. D. Pirone, N. A. G. Bandeira, B. Tylkowski, E. Boswell, R. Labeque, R. Garcia Valls, M. Giamberini, *Polymers* **2020**, *12*, 1019

55. a) R. Izsák, *WIREs Comput. Mol. Sci.* **2020**, *10*:e1445; b) R. Berraud-Pache, F. Neese, G. Bistoni, R. Izsák *J. Chem. Theory Comput.* **2020**, *16*, 564–575; c) A. Sirohiwal, R. Berraud-Pache, F. Neese, R. Izsák, D. A. Pantazis *J. Phys. Chem. B* **2020**, *124*, 8761–8771.
56. M. H. Lechner, F. Neese, R. Izsák, *Mol. Phys.* **2021**, *119*, e1965235.